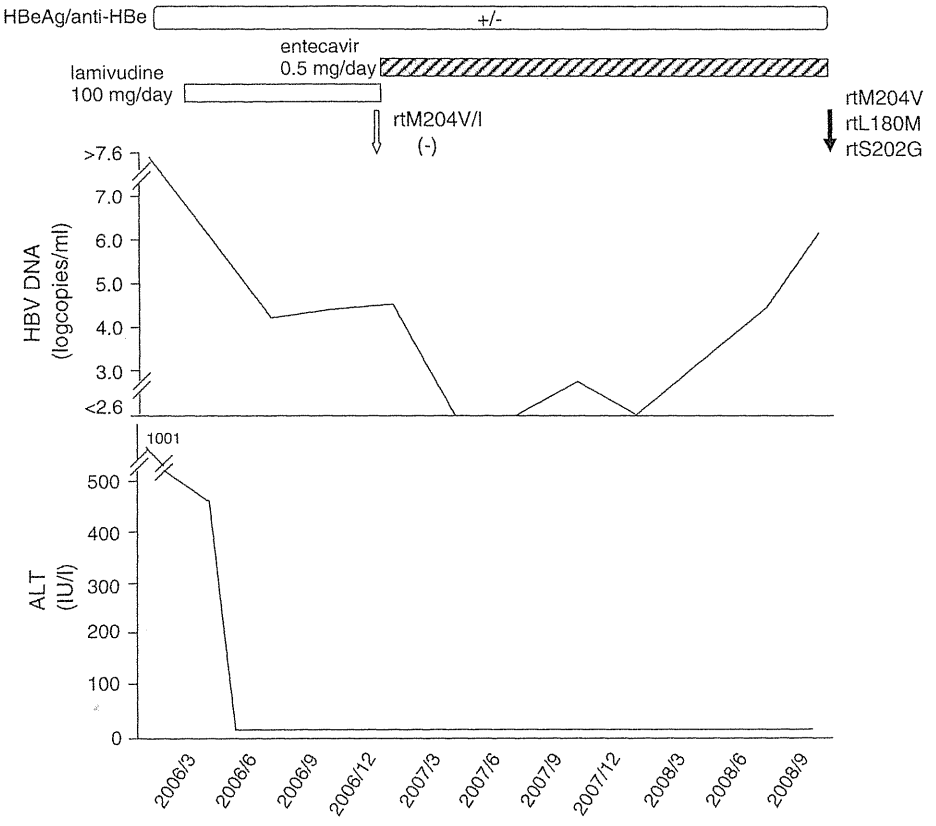

Fig. 2 Disease course of the CH-B patient showing entecavir-resistance during switching treatment to entecavir. The *white arrow* indicates the time point of the PCR–ELMA assay to detect rtM204V/I mutation, whereas the *black arrow* indicates the time point of the PCR-direct sequencing analysis

lamivudine treatment. In addition, the switching treatment to entecavir tended to yield a greater decrease in HBV DNA than the preceding lamivudine treatment. These results indicate that the switch from lamivudine to entecavir may be generally recommendable compared with continuation of lamivudine administration in CH-B patients without evidence of lamivudine resistance.

In this study, one of the six patients having baseline HBV DNA $\geq$4.0 logcopies/ml showed entecavir-resistance during the switching treatment to entecavir. It was probably due to the existence of an extremely small amount of lamivudine-resistant virus mixed with a predominant wild-type virus, which could not be detected by the sensitive PCR–ELMA assay at the start of the switch to entecavir treatment. It is speculated that, during entecavir treatment, the lamivudine-resistant virus having rtM204V and rtL180M substitutions may become predominant with time, followed by the establishment of entecavir-resistant virus via the additional rtS202G substitution. Compared to the low incidence of drug resistance in entecavir treatment for nucleos(t)ide analog-naïve CH-B patients [17], the entecavir-resistance may occur more frequently in the lamivudine-to-entecavir switching treatment for patients without evidence of lamivudine resistance. In particular, patients who do not achieve a good response to the preceding lamivudine treatment are speculated to have a higher risk for the development of entecavir-resistance in the switching treatment to entecavir, although it should be verified by further studies.

In conclusion, in CH-B patients receiving the continuous lamivudine treatment, it may be recommendable to switch to entecavir treatment before the appearance of lamivudine resistance. It may contribute to reducing the subsequent emergence of drug resistance. However, great care should be taken with respect to the emergence of entecavir-resistant virus after the switch to entecavir treatment, especially in patients who do not respond well to the preceding lamivudine treatment. Our retrospective study with a small number of patients and a short duration of follow-up cannot draw a definite conclusion but still provides some information about the clinical possibilities of the lamivudine-to-entecavir switching treatment. Further detailed investigation with a larger number of patients and a longer follow-up period may offer better understanding.

References

1. Lai CL, Chien RN, Leung NW, Chang TT, Guan R, Tai DI, et al. A one-year trial of lamivudine for chronic hepatitis B. Asia Hepatitis Lamivudine Study Group. N Engl J Med. 1998;339:61–8.
2. Dienstag JL, Schiff ER, Wright TL, Perrillo RP, Hann HW, Goodman Z, et al. Lamivudine as initial treatment for chronic

hepatitis B in the United States. N Engl J Med. 1999;341:1256–63.
3. Lai CL, Dienstag J, Schiff E, Leung NW, Atkins M, Hunt C, et al. Prevalence and clinical correlates of YMDD variants during lamivudine therapy for patients with chronic hepatitis B. Clin Infect Dis. 2003;36:687–96.
4. Allen MI, Deslauriers M, Andrews CW, Tipples GA, Walters KA, Tyrrell DL, et al. Identification and characterization of mutations in hepatitis B virus resistant to lamivudine. Lamivudine Clinical Investigation Group. Hepatology. 1998;27:1670–7.
5. Liaw YF, Chien RN, Yeh CT, Tsai SL, Chu CM. Acute exacerbation and hepatitis B virus clearance after emergence of YMDD motif mutation during lamivudine therapy. Hepatology. 1999;30:567–72.
6. Westland CE, Yang H, Delaney WE 4th, Wulfsohn M, Lama N, Gibbs CS, et al. Activity of adefovir dipivoxil against all patterns of lamivudine-resistant hepatitis B viruses in patients. J Viral Hepat. 2005;12:67–73.
7. Ono-Nita SK, Kato N, Shiratori Y, Lan KH, Yoshida H, Carrilho FJ, et al. Susceptibility of lamivudine-resistant hepatitis B virus to other reverse transcriptase inhibitors. J Clin Invest. 1999; 103:1635–40.
8. Hadziyannis SJ, Tassopoulos NC, Heathcote EJ, Chang TT, Kitis G, Rizzetto M, et al. Adefovir dipivoxil for the treatment of hepatitis B e antigen-negative chronic hepatitis B. N Engl J Med. 2003;348:800–7.
9. Marcellin P, Chang TT, Lim SG, Tong MJ, Sievert W, Shiffman ML, et al. Adefovir dipivoxil for the treatment of hepatitis B e antigen-positive chronic hepatitis B. N Engl J Med. 2003; 348:808–16.
10. Perrillo R, Hann HW, Mutimer D, Willems B, Leung N, Lee WM, et al. Adefovir dipivoxil added to ongoing lamivudine in chronic hepatitis B with YMDD mutant hepatitis B virus. Gastroenterology. 2004;126:81–90.
11. Peters MG, Hann Hw H, Martin P, Heathcote EJ, Buggisch P, Rubin R, et al. Adefovir dipivoxil alone or in combination with lamivudine in patients with lamivudine-resistant chronic hepatitis B. Gastroenterology. 2004;126:91–101.
12. van Bömmel F, Wünsche T, Mauss S, Reinke P, Bergk A, Schürmann D, et al. Comparison of adefovir and tenofovir in the treatment of lamivudine-resistant hepatitis B virus infection. Hepatology. 2004;40:1421–5.
13. van Bömmel F, Zöllner B, Sarrazin C, Spengler U, Hüppe D, Möller B, et al. Tenofovir for patients with lamivudine-resistant hepatitis B virus (HBV) infection and high HBV DNA level during adefovir therapy. Hepatology. 2006;44:318–25.
14. Chang TT, Gish RG, de Man R, Gadano A, Sollano J, Chao YC, et al. A comparison of entecavir and lamivudine for HBeAg-positive chronic hepatitis B. N Engl J Med. 2006;354:1001–10.
15. Lai CL, Shouval D, Lok AS, Chang TT, Cheinquer H, Goodman Z, et al. Entecavir versus lamivudine for patients with HBeAg-negative chronic hepatitis B. N Engl J Med. 2006;354:1011–20.
16. Sherman M, Yurdaydin C, Sollano J, Silva M, Liaw YF, Cianciara J, et al. Entecavir for treatment of lamivudine-refractory, HBeAg-positive chronic hepatitis B. Gastroenterology. 2006;130:2039–49.
17. Colonno RJ, Rose R, Pokornowski K, Baldick C, Eggers B, Yu D, et al. Four year assessment of ETV resistance in nucleoside-naïve and lamivudine refractory patients. J Hepatol. 2007; 46:S294. (Abst.).
18. Tenney DJ, Rose RE, Baldick CJ, Levine SM, Pokornowski KA, Walsh AW, et al. Two-year assessment of entecavir resistance in Lamivudine-refractory hepatitis B virus patients reveals different clinical outcomes depending on the resistance substitutions present. Antimicrob Agents Chemother. 2007;51:902–11.
19. Levine S, Hernandez D, Yamanaka G, Zhang S, Rose R, Weinheimer S, et al. Efficacies of entecavir against lamivudine-resistant hepatitis B virus replication and recombinant polymerases in vitro. Antimicrob Agents Chemother. 2002;46:2525–32.
20. Kobayashi S, Ide T, Sata M. Detection of YMDD motif mutations in some lamivudine-untreated asymptomatic hepatitis B virus carriers. J Hepatol. 2001;34:584–6.
21. Ono Y, Onda H, Sasada R, Igarashi K, Sugino Y, Nishioka K. The complete nucleotide sequences of the cloned hepatitis B virus DNA; subtype adr and adw. Nucleic Acids Res. 1983; 11:1747–57.
22. Fujiyama A, Miyanohara A, Nozaki C, Toneyama T, Ohtomo N, Matsubara K. Cloning and structural analyses of hepatitis B DNAs, subtype *adr*. Nucleic Acids Res. 1983;11:4601–10.
23. Kobayashi M, Koike K. Complete nucleotide sequence of hepatitis B virus DNA of subtype adr and its conserved gene organization. Gene. 1984;30:227–32.

BioSystems 99 (2010) 70–78

Contents lists available at ScienceDirect

BioSystems

journal homepage: www.elsevier.com/locate/biosystems

Reproducibility and usability of chronic virus infection model using agent-based simulation; comparing with a mathematical model

Jun Itakura[a,*], Masayuki Kurosaki[a], Yoshie Itakura[a], Sinya Maekawa[b], Yasuhiro Asahina[a], Namiki Izumi[a], Nobuyuki Enomoto[b]

[a] Division of Gastroenterology and Hepatology, Musashino Red Cross Hospital, 1-26-1 Kyonan-cho, Musashino-shi, Tokyo 180-8610, Japan
[b] First Department of Internal Medicine, Faculty of Medicine, University of Yamanashi, 1110, Shimogatou, Chuou-shi, Yamanashi 409-3898, Japan

ARTICLE INFO

Article history:
Received 30 June 2009
Received in revised form 27 August 2009
Accepted 6 September 2009

Keywords:
Agent-based model
Virus infectious disease

ABSTRACT

We created agent-based models that visually simulate conditions of chronic viral infections using two software. The results from two models were consistent, when they have same parameters during the actual simulation. The simulation results comprise a transient phase and an equilibrium phase, and unlike the mathematical model, virus count transit smoothly to the equilibrium phase without overshooting which correlates with actual biology in vivo of certain viruses. We investigated the effects caused by varying all the parameters included in concept; increasing virus lifespan, uninfected cell lifespan, uninfected cell regeneration rate, virus production count from infected cells, and infection rate had positive effects to the virus count during the equilibrium period, whereas increasing the latent period, the lifespan-shortening ratio for infected cells, and the cell cycle speed had negative effects. Virus count at the start did not influence the equilibrium conditions, but it influenced the infection development rate. The space size had no intrinsic effect on the equilibrium period, but virus count maximized when the virus moving speed was twice the space size. These agent-based simulation models reproducibly provide a visual representation of the disease, and enable a simulation that encompasses parameters those are difficult to account for in a mathematical model.

1. Introduction

All viruses need hosts as a basis for their life. When a virus enters the host body, it invades cells and uses both its own enzymes and those of the host cells to replicate. Host cells infected by viruses launch a self-defense system known as the innate immune system (See and Wark, 2008; Naniche, 2009), which inhibits viral replication and uses the human leukocyte antigen system and cytokines to elicit an immune response. Immune cells that have received signals from host cells activate other immune cells, neutralize viruses in the serum by means of antibodies, and prevent the virus from replicating and proliferating by destroying or curing host cells. Viral infection is a disorder based on the interactions between viruses and cells.

The power relationship between these agents changes along with the progression of the disease. In the very early stages of infection, as the host defense mechanisms are immature, the virus has the ability to overwhelm the host cells, actively replicate, and proliferate. Subsequently, as the capacity of the immune system improves, the speed of viral proliferation drops and the virus count reaches a peak. Infected host cells begin to be disrupted by the immune system or virus particles, and symptoms appear as a result. If the immune system is stronger than the virus, then the viral counts decline, and, in transient viral disorders, the virus is finally eliminated and the host recovers. In chronic viral disorders, however, the power relationship between the virus and host cells reaches equilibrium, and a long-term power balance is maintained with the virus count reaching a plateau.

Mathematical models have been proposed to study the dynamics of such viral disorders, and are regarded as being of value in understanding this phenomenon (Ho et al., 1995; Nowak et al., 1996; Neumann et al., 1998). However, these models are difficult to understand for clinicians, and their applicability is somewhat limited in everyday practice. In clinical research, measurements of viral dynamics in patients for short duration have been made for human

Abbreviations: HIV, human immunodeficiency virus; HBV, hepatitis B virus; HCV, hepatitis C virus.

* Corresponding author. Tel.: +81 422 32 3111; fax: +81 422 32 9551.
E-mail address: jitakura@musashino.jrc.or.jp (J. Itakura).

0303-2647/$ – see front matter © 2009 Elsevier Ireland Ltd. All rights reserved.
doi:10.1016/j.biosystems.2009.09.001

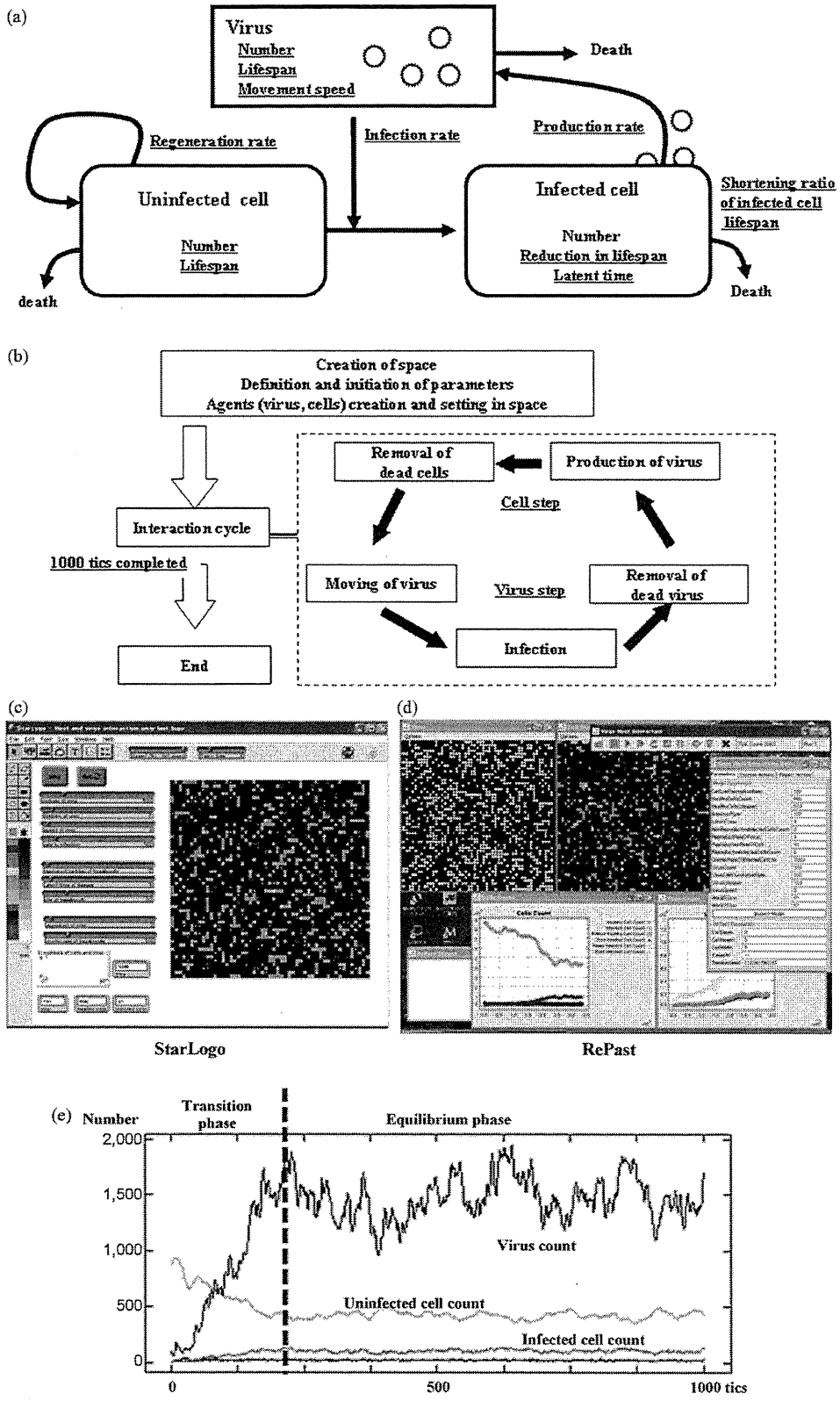

Fig. 1. Simulation design and an example of simulation results. (a) Model concept. Viruses, uninfected cells, and infected cells were treated as agents, and parameters were set for each of these and for interactions between agents (underlined). (b) Flowchart of the program. After preparing the simulation, we entered the interaction cycle, in which virus steps (such as movement) and cell steps were repeated. One cycle was counted as 1 tic, and the simulation concluded after 1000 tics. (c and d) Simulation screen using (c) StarLogo and (d) RePast. Yellow circles are viruses, green squares are uninfected cells, and orange and red indicate infected cells, with orange indicating the latent period. In StarLogo, all the agents are shown on the same screen, but in RePast, viruses and cells are shown in separate windows. (e) Example of a simulation chart in StarLogo. After the start of simulation the virus count and infected cell count increase while the uninfected cell count decreases, with equilibrium state reached after a certain number of tics.

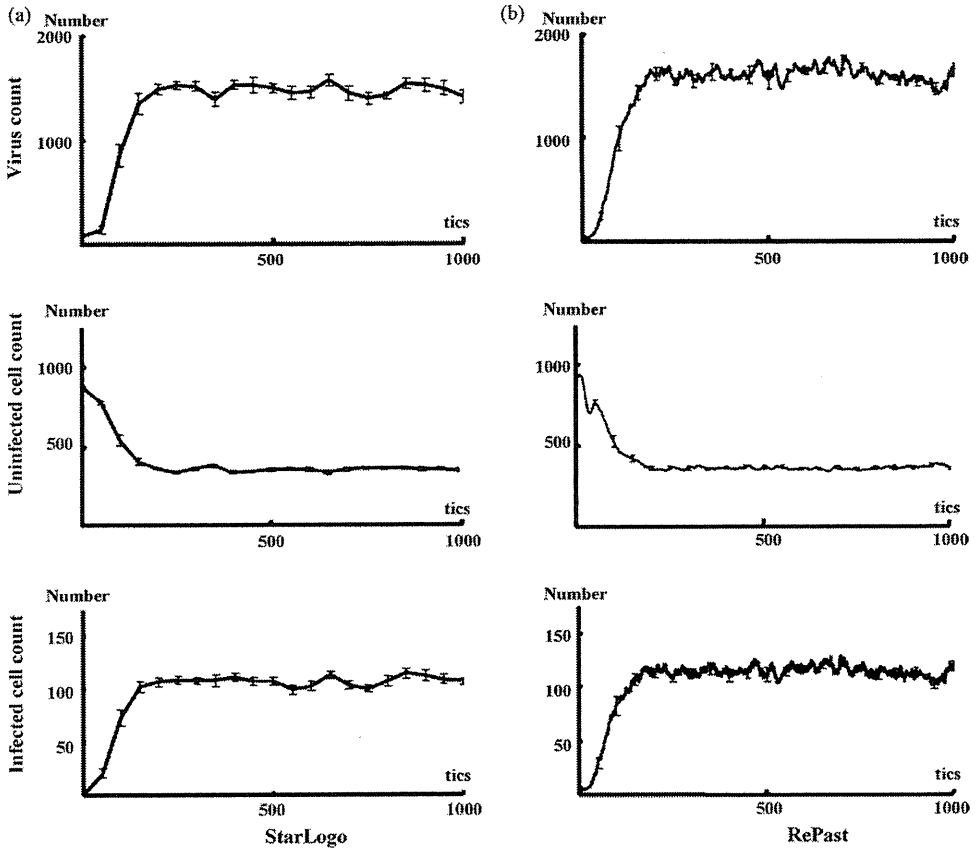

Fig. 2. Comparison of simulation results in (a) StarLogo and (b) RePast. The results were consistent when the parameters were made consistent. (Virus count [average ± SD]: StarLogo 1458.03 ± 173.1, RePast 1462.71 ± 178.8, $p = 0.94$. Uninfected cell count: 364.24 ± 30.4, 368.11 ± 33.4, $p = 0.83$. Infected cell count: 105.73 ± 13.0, 107.74 ± 13.0, $p = 0.24$. Unpaired Student's *t*-test.) Parameter values were set as follows: initial virus count, 100; uninfected cell count, 880; infected cell count, 0; virus speed of movement, 5 grids/tic; infection rate, 10%; uninfected cell regeneration rate, 1%; latent period, 3 tics; and virus reproduction rate, 5/cells/tic. The following parameter settings were taken from actual measurements: virus lifespan, 4.5 tics; uninfected cell lifespan, 49.8 tics; and infected cell lifespan, 6.7 tics.

immunodeficiency virus (HIV) (Ho et al., 1995), hepatitis B virus (HBV) (Nowak et al., 1996) and hepatitis C virus (HCV) (Neumann et al., 1998), and research is also underway on a range of models based on animal experiments and cell culture systems. As chronic viral disorders persist over long periods of time complete follow-up of viral dynamics is difficult. Furthermore, limitations of items that can be measured, such as the difficulty of measuring whole numbers of host cells, make it extremely difficult to investigate their consistency in mathematical models.

The recent ascend of dynamic-models owes much to advances in computers. Computer performance has improved markedly in recent years, not only in terms of their calculating capacity but also with regard to image displays, and models that offer a visual representation of viral disorders are now being reported (Gilbert and Bankes, 2002; Duca et al., 2007; Shapiro et al., 2008; Castiglione et al., 2007). One advantage of such visual models is that by providing a visual representation, they make understanding the disease status easy. Another benefit is that they enable parameters to be identified that are hidden as background noise in mathematical models. However, these models have some problems; it is difficult to prove the reproducibility of the simulation results derived from different languages or libraries, difficult to prove the validity of the model's concepts, and difficult to prove that the simulation results accurately reflect the reality. In this study, we created agent-based computer models that visually simulate the conditions of chronic viral infections using two software. The reproducibility of two agent-based computer models and the differences between agent-based models and the mathematical model were analyzed. This agent-based model enabled us to investigate how each parameter included in the concept affects the conditions of chronic viral infections.

2. Methods

2.1. Selection of Software

In this study, we used two different types of softwares: StarLogo version 2.0 (http://education.mit.edu/starlogo/) supplied by MIT Media Laboratory and Recursive Porous Agent Simulation Toolkit (RePast-3.0, http://repast.sourceforge.net/) supplied by the Argonne National Laboratory. StarLogo uses Logo, one of the simplest programming languages, and has a fixed graphical user interface. RePast is a library that uses Java, another programming language, which also has a fixed graphical user interface.

Logo is an assembly language, and StarLogo carries out processing sequentially. Java is an object-oriented language, and RePast has a faster processing speed than StarLogo. In addition, StarLogo has a number of stipulations to simplify simulations, such as parameters can only be set up to five decimal places and the simulation space is also fixed as 51×51 square grids. RePast, on the other hand, has fewer such restrictions. Thus, it offers a higher degree of freedom in program settings than StarLogo. Taking simulation space as an example, in spite of the restrictions imposed by the underlying operating system's image display system, any number of grids can be set and a hexagonal grid could also be chosen rather than a square one. However, users must stipulate and set all parameters themselves. This means that they must first declare the shape of the grid and the number of grids they will use to fill the simulation space. Java is also more difficult to learn than Logo, and debugging and correcting the program is also more difficult. Thus, it is difficult to judge whether or not the results agree with the planned simulation.

In effect, these two different types of softwares are polar opposites. It is simple to start a simulation in StarLogo, but producing results takes time and it is difficult to carry out more complex simulations. In RePast it is difficult to compose the program and judge whether or not the planned study has actually been achieved, but the

simulation itself takes only a short time to complete and there are lesser restrictions in the construction of a simulation model.

2.2. Concept for Modeling

We applied the basic virus–host interaction mathematical model to the agent-based simulation system with slight modifications. The mathematical model was used to describe the dynamics of HIV (Ho et al., 1995), HBV (Nowak et al., 1996), and HCV (Neumann et al., 1998) and the only agents involved were host cells and viruses, without the inclusion of immune cells. The effects of the immune system are expressed by varying parameters such as lifespan of host cells and viruses.

Fig. 1a illustrates the study concept. Viruses have the ability to infect healthy host cells (uninfected cells) and the infected cells produce new viruses. Both cells and viruses have definite lifespans, and the lifespan of infected cells is usually shorter than that of uninfected cells. Uninfected cells automatically regenerate within the space, whereas infected cells only arise due to infection of uninfected cells. Viruses also lack the ability to regenerate themselves and are only produced from infected cells.

2.3. Parameter Settings

In the present study, as the StarLogo settings are circumscribed, we limited the simulation space to 51 × 51 square grids. However, we made an exception here while investigating the effects of size of space on the simulation results. The numbers of viruses, uninfected cells, and infected cells could only be set before the start of the simulation. As described in the later, our simulation ran in cycles, with 1 cycle defined as 1 tic.

In mathematical simulation models, the death rate is required as a parameter. However, in our program we set lifespans for viruses and uninfected cells. These lifespans were not uniform, but were set to have a deviation of about 10%. The lifespan of cells was shortened by infection with ratio decided beforehand.

The infection ratio was meaningful only when an infected cell and a virus coincidentally occupied the same grid, and this was used to calculate the probability of the infection occurring in that situation. The virus production rate was set as the number of viruses produced by an infected cell during 1 tic. Infected cells could be set as a parameter indicating the latent period between the time of virus infection and the time of virus replication.

In order to emulate the tissue repair capacity, we set uninfected cell regeneration rate such that grids without any cells had a specified probability of producing uninfected cells on top of themselves. As a result, the more the cell count declined within a space the more regenerated uninfected cells were produced, whereas the number of regenerated cells declined as cell count increased.

The number of grids through which a virus could move in 1 tic was set as the speed of movement, and the direction of movement was set within a range of 90° toward the top of the simulation space. The program used a circulatory method of movement; when a virus arrived at the top of the space, it was translocated to the bottom, and moved again toward the top. Cells were fixed on the grid.

2.4. Simulation Flowchart

Fig. 1b shows a flowchart of the program. First, the simulation space was produced, after which each parameter was defined and the initial settings were made. Next the agents – viruses and uninfected and infected cells – were produced. The simulation cycle was as follows. Viruses moved to a new grid, and if an uninfected cell was present, this was infected with a probability based on the infection rate. The lifespan of the virus decreased, and viruses that had completed their lifespan and those that had caused an infection were removed from the space. Infected cells produced new viruses, the lifespans of both uninfected and infected cells decreased. Then, cells that had completed their lifespan were eliminated and a new cycle began. The program was set such that the simulation ended after this cycle had repeated 1000 times. This meant that one simulation was complete after 1000 tics.

2.5. Data Collection

The RePast model was programmed such that data for each tic was saved automatically as a text file at the end of the simulation. This text file could be opened by a database software. The StarLogo model was programmed to stop the simulation and collect data after every 50 tics.

2.6. Mathematical Model

In order to compare the results of this agent-based simulation, we used a viral infection mathematical model, which we improved as follows.

$$\frac{dT}{dt} = s[2601 - (T + I)] - dT - bVT \quad (1)$$

$$\frac{dI}{dt} = bVT - dI \quad (2)$$

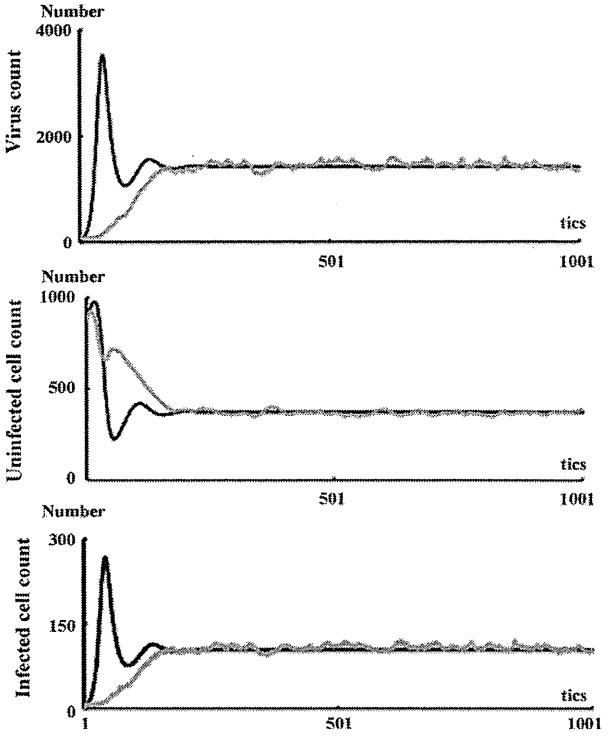

Fig. 3. Comparison of results of agent-based simulation and mathematical simulation. Both sets of results were consistent for the equilibrium phase, but differed in the shift in transition phase. Black line: mathematical model; grey line: results of simulation in RePast. Parameter values were set as follows: initial virus count, 100; uninfected cell count, 880; infected cell count, 0; virus speed of movement, 5 grids/tic; infection rate, 10%; uninfected cell regeneration rate, 1%; latent period, 3 tics; virus reproduction rate, 5/cells/tic; virus lifespan, 10 tics; uninfected cell lifespan, 50 tics; and cell lifespan-shortening ratio as a result of infection, 69%.

$$\frac{dV}{dt} = pI - cV \quad (3)$$

where, T is the uninfected cell count, I is the infected cell count, and V is the virus count. Uninfected cells are supplied to the space with a probability $s[2601 - (T+I)]$, as the number of grids in this agent-based simulation model was 2601 (51 × 51). The death rate of uninfected cells is d, the death rate of infected cells is δ, and the death rate of viruses is c. The infection rate is indicated by β. Viruses are released from infected cells at a probability p.

2.7. Statistical Analysis

Statistical analyses were performed by statistical tests using the program StatView 5.0 (SAS Institute Inc.). All tests of significance were two-tailed, with p values of <0.05 considered to be significant.

3. Results

3.1. Reproducibility of Chronic Viral Infection Disease Models Using Agent-based Simulation Methods

We constructed the chronic viral infection model with StarLogo library. Fig. 1c shows the simulation screen, and Fig. 1e shows one sample result. Immediately after the start of the simulation, the virus count temporarily dropped in accordance with the onset of an infection. Subsequently, the virus count started to increase with an increase in the infected cells and a decrease in the uninfected cells. After a certain number of tics (around 300 in this example), although the virus count, infected cell count, and uninfected cell count had some fluctuation, an equilibrium state was reached. We use the following descriptive terms in this paper: the transient phase is the period during which virus growth peaks, and the equilibrium phase is the period during which an equilibrium state is

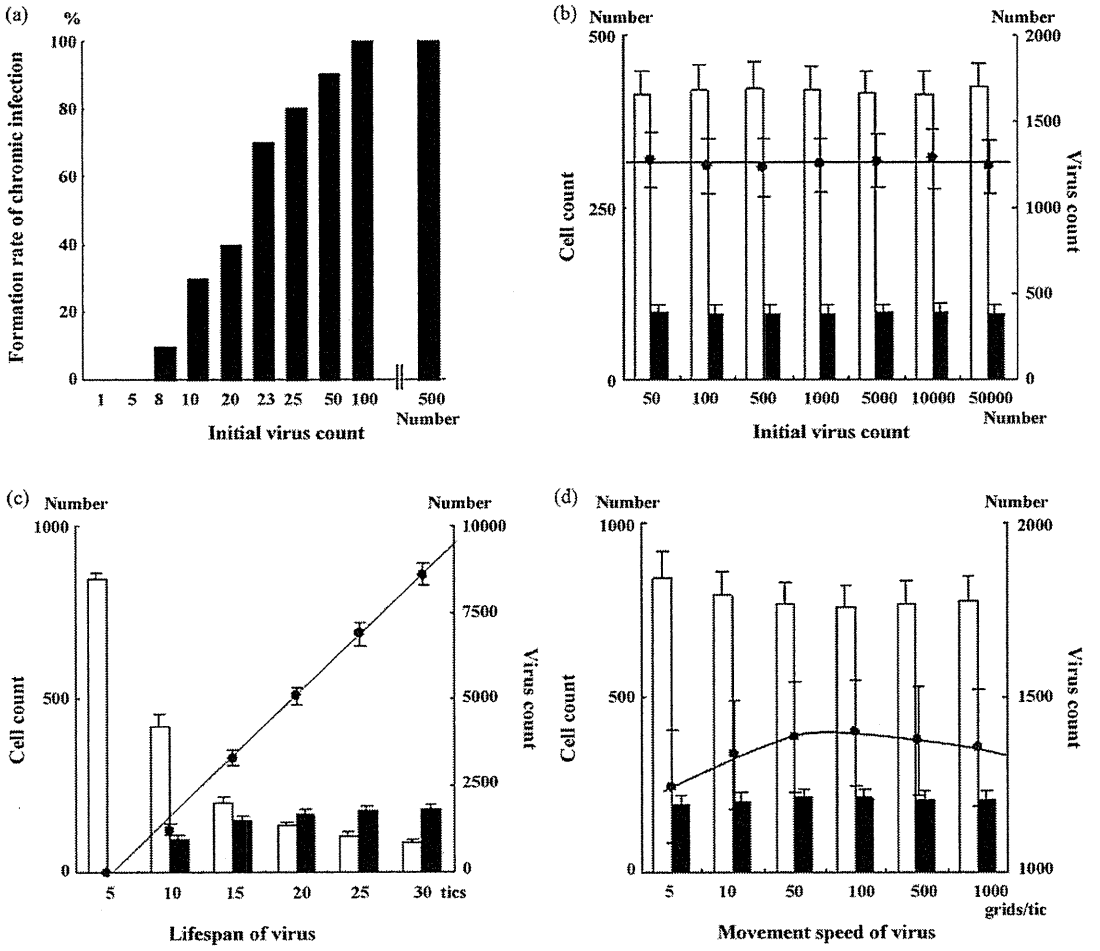

Fig. 4. Effects of changes in viral parameters. (a) The higher the initial virus count, the greater is the increase in the rate of formation of chronic infection, but (b) there was no effect on the conditions in the equilibrium phase. (c) Extending the virus lifespan increased the virus count. (d) Increasing the speed of virus movement to 100 grids/tic increased the virus count, but increasing it to 500 grids/tic had the opposite effect, with a slight declining trend. (a) Black bars: number of infections produced; (b–d) black circles: virus count; line: virus count approximation curve; white bars: uninfected cell count; black bars: infected cell count.

established. When the simulation was performed multiple times, the features described above were maintained, and the average values for virus, infected cell, and uninfected cell counts during the equilibrium state were all consistent.

Fig. 1d shows the simulation screen of the RePast. When we attempted setting all the initial parameters to the same values as those in the StarLogo, the results were not consistent. When we recalculated the parameters from the simulation results, in RePast, the parameters were largely maintained at the levels of the settings, but in StarLogo, the lifespans of both cell types became shorter than the settings while the simulation was in progress. We made the results of both simulations consistent by using the same parameters during the actual simulation (Fig. 2a and b).

3.2. Comparison Between Agent-based Simulation Models and Mathematical Simulation Model

We investigated whether the results of a chronic viral infection disease model produced by RePast would be consistent with the results of a mathematical model. For the mathematical model, we carried out an approximate integration using a four-dimensional Runge–Kutta method to ensure that the uninfected cell count and infected cell count would be in the same class. Parameters were always fixed as constant between simulations. The simulation results were consistent for the equilibrium phase, but transitions in virus count during the transient phase varied, with a shift to equilibrium state following two overshoots in the mathematical model, but a monotonic increase following a logistic curve in the agent-based model (Fig. 3). In the mathematical model, when the equilibrium condition was calculated with $dT/dt = dI/dt = dV/dt = 0$, the equilibrium-phase virus count, uninfected cell count, and infected cell count were very similar to those of the agent-based model (virus count: mathematical model 371.8/space, agent-based model 371.1 ± 32.4/space [average $\pm$ SD]; uninfected cell count: mathematical model 1605/space, agent-based model 1454 ± 194/space; infected cell count: mathematical model 115.9/space, agent-based model 108.3 ± 14.2/space).

3.3. Usability of the Models; Effect of Changing Parameters

We investigated the changes in the equilibrium phase brought about by changing each parameter. All the investigations below were carried out by using RePast, and we used the average values from ten simulations.

3.4. Viral Parameters

The lower the virus counts at the beginning of the simulation, the lower the probability of a chronic infection (Fig. 4a). However, the initial virus count did not have any effect on the equilibrium

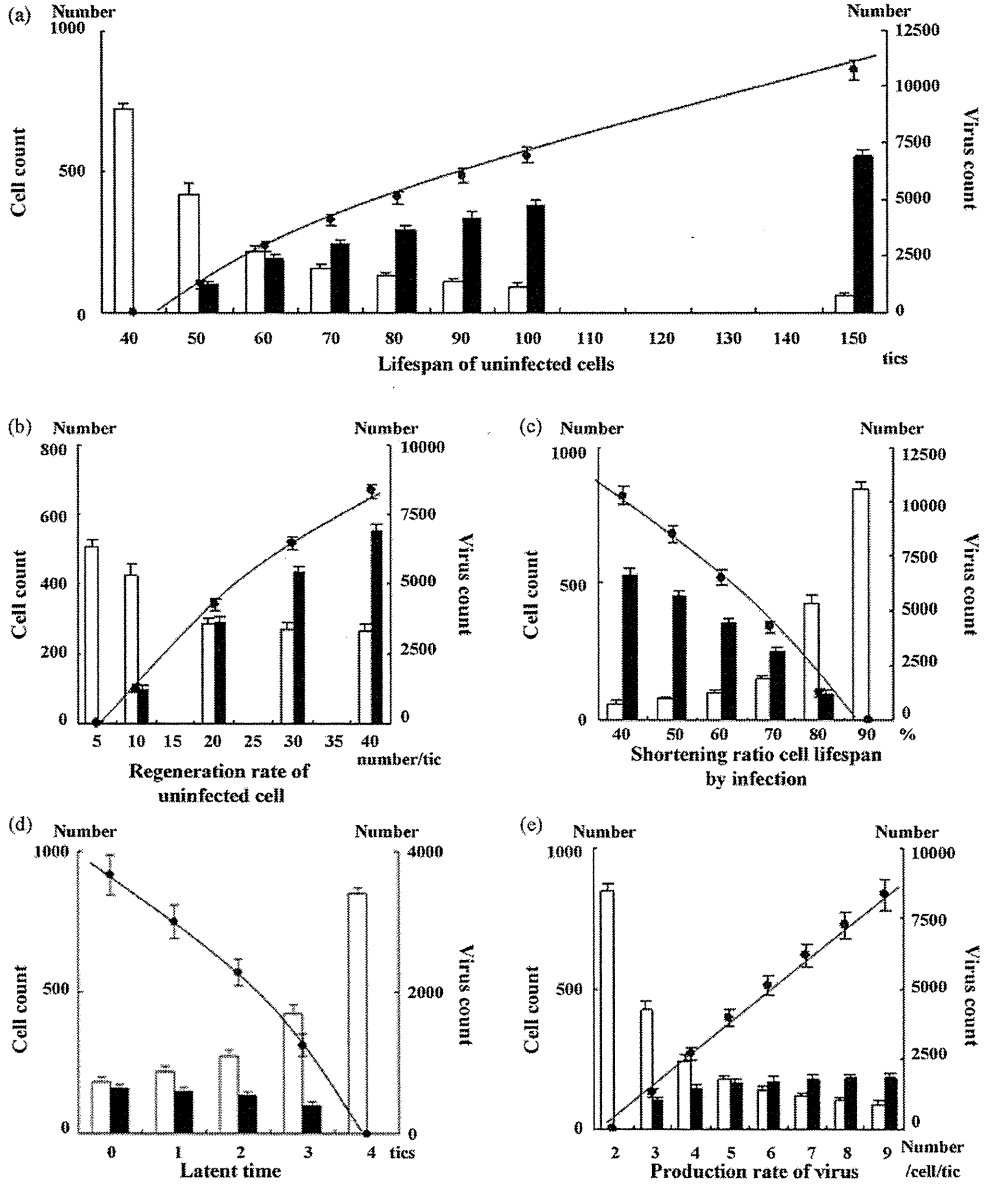

Fig. 5. Effects of changes in cell parameters. (a) Extending the uninfected cell lifespan and (b) increasing the uninfected cell regeneration rate increased the virus count. (c) Raising the lifespan-shortening ratio as a result of infection shortened the lifespan of infected cells, thereby decreasing the virus count. (d) Extending the latent period shortened the period of virus production from infected cells, thereby decreasing the virus count. (e) Increasing the virus production count resulted in a linear increase in equilibrium-phase virus count. Black circles: virus count; line: virus count approximation curve; white bars: uninfected cell count; black bars: infected cell count.

phase itself (Fig. 4b). Extending the lifespan of viruses resulted in a linear increase in equilibrium-phase virus count (Fig. 4c). Although the infected cell count increased, the rate of increase gradually declined. Changing the speed of viral movement resulted in the equilibrium-phase virus count to eventually decline after 100 grids/tic was reached, allowing movement over an area twice the size of the simulation space (Fig. 4d).

3.5. Uninfected Cell Parameters

Extending the lifespan of uninfected cells led to an increased virus count during the equilibrium phase (Fig. 5a). Increasing the uninfected cell regeneration rate also contributed to increased equilibrium-phase virus count (Fig. 5b). In both the cases, the increases in virus count and infected cell count were not linear, but showed a tendency for the rate of increase to decline gradually.

3.6. Infected Cell Parameters

We carried out an investigation of the effects of variation in the lifespan-shortening ratio on the virus count on the assumption that cell lifespan is shortened by infection. When this ratio was increased, the virus count decreased (Fig. 5c). An extended latent period was also related to a decreased virus count (Fig. 5d). However, the virus production from infected cells led to a linear increase in the virus count (Fig. 5e).

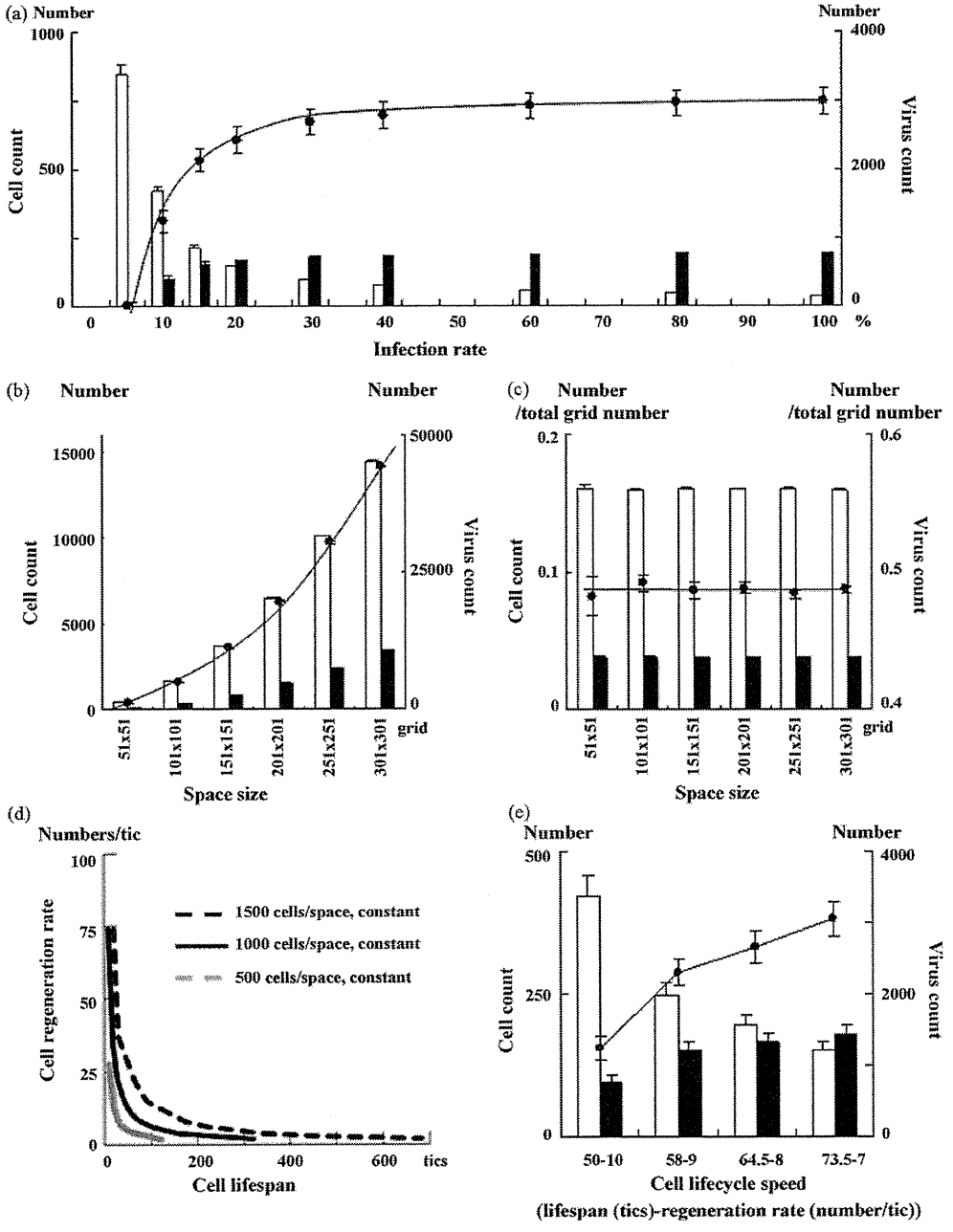

Fig. 6. (a) Increasing the infection rate increased the virus count in equilibrium periods, but the virus count did not change at infection rates of 30% or more. (b) The size of the simulation space increased not only virus count but also the cell count; however, (c) when virus and cell counts were divided by the total number of grids in the space, they were constant for all space sizes. (d) Changing the lifespan and regeneration rate of uninfected cells in opposite directions at the same time makes it possible to change only the cell cycle speed without altering the uninfected cell count. (e) When the cell cycle speed was reduced, the virus count increased toward the right of the graph. This may be because the effect of extending the lifespan of cells exceeds that of reducing their regeneration rate. (a–c and e) Black circles: virus count; line: virus count approximation curve; white bars: uninfected cell count; black bars: infected cell count.

3.7. Infection Rate and Space Size

Increasing the infection rate caused an increase in the virus count, but the change was minimal at an infection rate of 30% or more. The same results were seen for infected cell count, but a decrease in uninfected cell count resulted in a tendency for the infection rate to decrease by up to 60% (Fig. 6a).

The larger the space, higher the increase in both virus and cell counts (Fig. 6b). This increase was proportional to space size, however, when virus and cell counts were divided by the total number of grids in the space they were all constant (Fig. 6c).

3.8. Cell Cycle Speeds

Running a simulation with the initial virus count set to zero enables only the equilibrium condition for uninfected cells to be simulated. Changing the lifespan and regeneration rate of uninfected cells in opposite directions at the same time makes it possible

to change the cell cycle speed without altering the uninfected cell count (Fig. 6d). We used this technique to investigate how changing the cell cycle speed affected the equilibrium phase. Fig. 6e shows the results. Cell lifespan increases while the cell cycle speed declines. The equilibrium virus count increased in accordance with slower cell cycle speeds.

4. Discussion

In this study, we investigated the models using two agent-based simulation methods to program a simple virus–host chronic infection model. The same model written in two different programming language systems displayed the same results. The transient phase was unlike that seen in a mathematical simulation with no overshoot in virus count, but rather a smooth transition to the equilibrium phase. The virus count at the start of the simulation only had effect on the rate of infection development. Increases in virus lifespan, uninfected cell lifespan, uninfected cell regeneration rate, virus production count from infected cells, and infection rate all led to increased equilibrium-phase virus count. Rises in the infected cell lifespan-shortening ratio, latent period, and cell cycle speed decreased the equilibrium-phase virus count. The size of the space itself had no innate effect on the equilibrium phase, but a speed of movement of the virus that was twice the size of the space produced the maximum virus count.

Reproducibility is the basis for all scientific study, but there are many problems to prove it in computer simulations, such as programming bugs. As agent-based simulation deals with numerous agents individually, it requires vast amounts of calculations. Accumulation of very small change of values leads to large differences of results. In this study, we investigated two programs based on two programming languages to confirm the reproducibility of our simulation results in different programming languages. The results of two simulations were consistent, but in StarLogo, the lifespan parameters had a tendency to be lower than when they were set while simulations were actually in progress. This may be because the number of digits used in calculations was different between the two programs. RePast performs calculations to at least eight decimal places. In StarLogo, the library settings only enable settings to be made up to five decimal places. It is probable that these small differences accumulate during repeated calculations and are reflected in the simulation. Ultimately, we confirmed that the differences in results obtained by using different libraries and programming languages were not innate and by making the parameters consistent during simulation, consistent results were obtained.

Mathematical models using formulae for HIV therapy was published in 1994, the method has since been applied to HBV and HCV (Ho et al., 1995; Nowak et al., 1996; Neumann et al., 1998), and they were thought to be good reflections of the reality. In the mathematical model, viruses and cells are conceived as individuals in the concept itself, but both of them are perceived *en masse* when calculations are performed. However a feature of the agent-based simulation is that it deals with individual viruses and cells as separate agents. By moving each agent individually, it probes the factors influencing overall shifts from the micro viewpoint. When the space is viewed as a whole, it is possible to watch on the screen the collective movement of groups of agents. Recently, models that provide a visual representation of Epstein-Barr virus and HIV infection have been reported, both of which are useful for an instinctive and intuitive understanding (Duca et al., 2007; Shapiro et al., 2008; Castiglione et al., 2007).

In agent-based simulation model, virus count transit smoothly to the equilibrium phase. On the other hand, virus counts overshoot during transient phase in mathematical model. We think this difference is derived from technicality of different modeling. The difference in concepts between mathematical models and agent-based models is the space. The mathematical model has no space in concept, but agents move across the space in the agent-based model. In agent-based models, the densities of virus and cells change overtime especially in the transition phase because of the limited space. These changes of the densities of virus and cells lead to the dynamic change of the encounter rate of viruses and cells. The mathematical model does not make such concept of the density; the encounter rate is constant. This may be the reason for the difference between two models in the transition phase. Since no overshoot of virus counts in transient phase had been reported from in vivo studies of hepatitis C virus and simian immunodeficiency virus (Dahari et al., 2005; Nowak et al., 1997), agent-based model correlates with actual biology in vivo at least for these viruses. The increase of initial virus count at the start of simulation correlates with higher encounter rate of viruses and cells which make the linear increasing of infection forming rate. Mathematical model can only express the infection formation rate as "infected or not".

The importance of viral passing speed in the agent-based model is also explained by the "space". Although the virus actually moves through the blood stream in our body and virus could not decide their moving speeds by themselves, there is most appropriate speed for virus to meet the cells on the simulation space by the highest probability. The effect of cell cycle speed should be mentioned by another affection of the space. A fast cell cycle speed means that the lifespan of uninfected cells is short. Then fast cell cycle speed leads to the short lifespan of infected cells. A higher regeneration rate for uninfected cells results in a higher rate of infection among uninfected cells by viruses, but in situations where viruses and cells are dispersed around the space this is ineffective in increasing the infection rate, as the latter depends on the probability that they will encounter one another. As a result, the infected cell count decreases during the equilibrium phase, as does the virus count.

In this study, we confirmed the reproducibility and usability of agent-based models in expressing the interaction between viruses and cells. A feature of this simulation system is that it uses the concept of space as actual space, which means that the existence of the space becomes an additional controlling factor on the simulation results. This is a concept that is absent from mathematical models. The reality is that we have a spatial existence, and an advantage of the agent-based simulation system is the fact that it accounts for the space. Another feature of the simulation system is that it enables the condition to be perceived in visual terms, making it easy to understand. However it may be affected by computer performance and by the limitations of programming languages or the program itself, this system may offer a powerful tool for the future analysis of real virus–host interaction disease.

Conflict of interest

No conflicts of interest exist for all authors.

References

Castiglione, F., Pappalardo, F., Bernaschi, M., Motta, S., 2007. Optimization of HAART with genetic algorithms and agent-based models of HIV infection. Bioinformatics 23, 3350–3355, doi:10.1093/bioinformatics/btm408.

Dahari, H., Major, M., Zhang, X., Mihalik, K., Rice, C.M., Perelson, A.S., Feinstone, S.M., Neumann, A.U., 2005. Mathematical modeling of primary hepatitis c infection: noncytolytic clearance and early blockage of virion production. Gastroenterology 128, 1056–1066, doi:10.1053/j.gastro.2005.01.049.

Duca, K.A., Shapiro, M., Delgado-Eckert, E., Hadinoto, V., Jarrah, A.S., Laubenbacher, R., Lee, K., Luzuriaga, K., Polys, N.F., Thorley-Lawson, D.A., 2007. A virtual look at Epstein-Barr virus infection: biological interpretations. PLoS Pathog. 3, 1388–1400, doi:10.1371/journal.ppat.0030137.

Gilbert, N., Bankes, S., 2002. Platforms and methods for agent-based modelling. Proc. Natl. Acad. Sci. U.S.A. 99 (Suppl. 3), 7197–7198.

Ho, D.D., Neumann, A.U., Perelson, A.S., Chen, W., Leonard, J.M., Markowitz, M., 1995. Rapid turnover of plasma virions and CD4 lymphocytes in HIV-1 infection. Nature 373, 123–126, doi:10.1038/373123a0.

Naniche, D., 2009. Human immunology of measles virus infection. Curr. Top. Microbiol. Immunol. 330, 151–171.

Neumann, A.U., Lam, N.P., Dahari, H., Gretch, D.R., Wiley, T.E., Layden, T.J., Perelson, A.S., 1998. Hepatitis C viral dynamics in vivo and the antiviral efficacy of interferon-alpha therapy. Science 282, 103–107, doi:10.1126/science.282.5386.103.

Nowak, M.A., Bonhoeffer, S., Hill, A.M., Boehme, R., Thomas, H.C., McDade, H., 1996. Viral dynamics in hepatitis B virus infection. Proc. Natl. Acad. Sci. U.S.A. 93, 4398–4402.

Nowak, M.A., Lloyd, A.L., Vasquez, G.M., Wiltrout, T.A., Wahl, L.M., Biscofberger, N., Williams, J., Kinter, A., Fauci, A.S., Hirsch, V.M., Lifson, J.D., 1997. Viral dynamics of primary viremia and antiretroviral therapy in simian immunodeficiency virus infection. J. Virol. 71, 7518–7525.

Shapiro, M., Duca, K.A., Lee, K., Delgado-Eckert, E., Hawkins, J., Jarrah, A.S., Laubenbacher, R., Polys, N.F., Hadinoto, V., Thorley-Lawson, D.A., 2008. A virtual look at Epstein-Barr virus infection: simulation mechanism. J. Theor. Biol. 252, 633–648, doi:10.1016/j.jtbi.2008.01.032.

See, H., Wark, P., 2008. Innate immune response to viral infection of the lungs. Paediatr. Respir. Rev. 9, 243–250, doi:10.1016/j.prrv.2008.04.001.

Digestive Endoscopy (2009) **21**, 67–72 doi:10.1111/j.1443-1661.2009.00844.x

REVIEW

LAPAROSCOPIC RADIOFREQUENCY ABLATION FOR HEPATOCELLULAR CARCINOMA

YASUHIRO ASAHINA, HIROYUKI NAKANISHI AND NAMIKI IZUMI

Division of Gastroenterology and Hepatology, Musashino Red Cross Hospital, Kyonan-cho, Musashino-shi, Tokyo, Japan

Radiofrequency ablation (RFA) is one of the best curative treatments for hepatocellular carcinoma in selected patients, and this procedure can be applied either percutaneously or laparoscopically. Although the percutaneous approach is less invasive and is considered the first choice, RFA with laparoscopic guidance is highly recommended for patients with a relative contraindication for percutaneous RFA, such as lesions adjacent to the gastrointestinal tract, gallbladder, bile duct and heart. Recent advances in laparoscopic ultrasound have widened the indication for laparoscopic ablation. In the present paper, we review the indications, advantages, prognosis and safety of laparoscopic RFA for hepatocellular carcinoma.

Key words: hepatocellular carcinoma, laparoscopic ultrasonography, laparoscopy, radiofrequency ablation.

INTRODUCTION

Hepatocellular carcinoma (HCC) is one of the most frequent primary hepatic malignancies, not only in Japan, but also in the USA and Europe.[1–4] HCC is closely linked to chronic liver diseases including hepatitis B and hepatitis C.[5] Surveillance of these patients can lead to an HCC diagnosis at an early stage, when the tumor may be cured with resection, liver transplantation or local ablation.[6–8] Unlike other solid tumors, surgical resection plays a limited role in the treatment of hepatocellular carcinoma,[7,9,10] because underlying cirrhosis or multiple lesions often contraindicate surgery. Furthermore, this cancer frequently recurs, even after apparently curative resection.[11] Liver transplantation may be effective in highly selected patients,[12] but its feasibility is restricted by the shortage of donors.[13,14] Hence, several alternative non-surgical treatments to potentially cure HCC have been developed.

Radiofrequency ablation (RFA), also known as radiofrequency thermal ablation, is a recently developed thermoablative technique.[15–18] It induces temperature changes by using high-frequency alternating current applied via electrodes placed within the tissue to generate areas of coagulative necrosis and tissue desiccation.[19,20] RFA can be applied percutaneously, laparoscopically or during open surgery.

In 1997, Curley *et al.* performed a feasibility study of laparoscopic RFA on pigs demonstrating the simplicity of the procedure,[21] and favorable results were subsequently achieved in preliminary clinical experience.[22–24] The laparoscopic approach has the benefits of direct visual control of the RFA procedure, exposure and isolation of the liver from the surrounding tissue, and effective management of intraoperative bleeding.[25]

Correspondence: Namiki Izumi, Division of Gastroenterology and Hepatology, Musashino Red Cross Hospital, 1-26-1 Kyonan-cho, Musashino-shi, Tokyo 180-8610, Japan. Email: nizumi@musashino.jrc.or.jp

Received 24 October 2008; accepted 5 January 2009.

INDICATIONS FOR LAPAROSCOPIC RFA AS A CURATIVE TREATMENT

The current indications for laparoscopic RFA as a curative therapy are similar to percutaneous RFA: three or fewer tumors measuring ≤3 cm in diameter, or a solitary tumor with a major axis of ≤5 cm and liver function of Child–Pugh class A or B. Although curative ablation is possible for tumors measuring ≤2 cm in diameter, there is no clear evidence that ablation can cure hypervascular HCC >3 cm in diameter. HCC with extrahepatic metastasis, and vascular or biliary invasion should be excluded from the indication.

Similar to percutaneous RFA, the contraindications for laparoscopic RFA are jaundice, refractory ascites, and a tendency for hemorrhage (platelet count $<50 \times 10^9$/L or prothrombin activity <50%). However, RFA with laparoscopic guidance is highly recommended for patients with a relative contraindication for percutaneous RFA, such as lesions adjacent to the gastrointestinal tract, gallbladder, bile duct or heart.[26] Contraindications specific to laparoscopic RFA are the same as for generic laparoscopy and include previous abdominal surgery, cardiopulmonary disorders and severe obesity.

LAPAROSCOPIC RFA PROCEDURE

Laparoscopic RFA is usually carried out under general anesthesia. After infusing carbon dioxide gas into the peritoneal cavity to generate a pneumoperitoneum, a laparoscope is inserted through a 5–10 mm trocar depending on its diameter. A mesh-covered access port (VersaStep®; US Surgical, Norwalk, CT, USA) is recommended to avoid arterial bleeding from the abdominal wall and to avoid visceral injury. After the endoscopic examination, a laparoscopic ultrasound probe is inserted through the second trocar to screen, detect and determine the puncture point for the tumor (Fig. 1). The RF electrode is inserted under ultrasonic guidance (Fig. 1), and ablation is carried out as many times as needed. Either an expandable electrode with a thermo-controlled generator

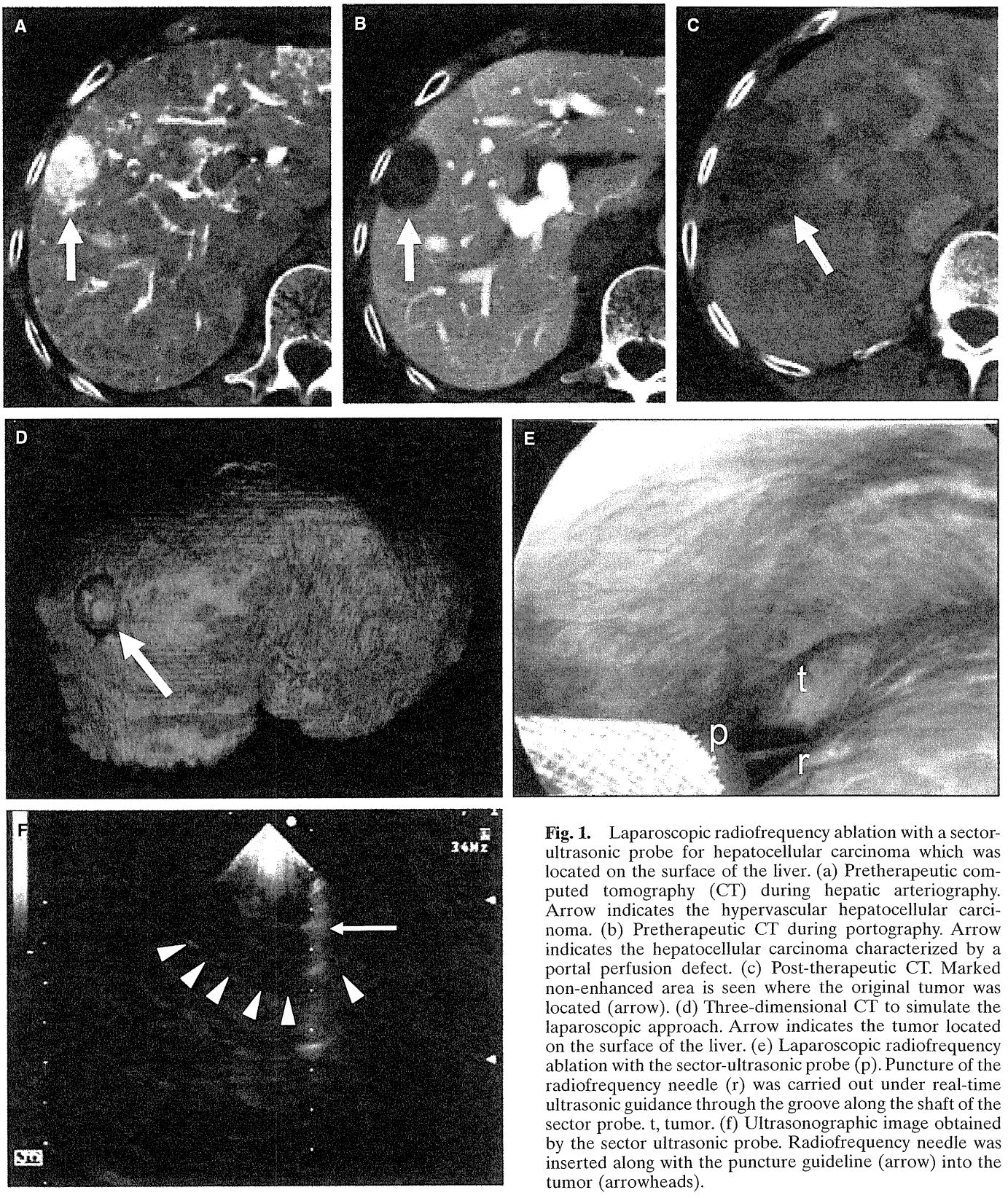

Fig. 1. Laparoscopic radiofrequency ablation with a sector-ultrasonic probe for hepatocellular carcinoma which was located on the surface of the liver. (a) Pretherapeutic computed tomography (CT) during hepatic arteriography. Arrow indicates the hypervascular hepatocellular carcinoma. (b) Pretherapeutic CT during portography. Arrow indicates the hepatocellular carcinoma characterized by a portal perfusion defect. (c) Post-therapeutic CT. Marked non-enhanced area is seen where the original tumor was located (arrow). (d) Three-dimensional CT to simulate the laparoscopic approach. Arrow indicates the tumor located on the surface of the liver. (e) Laparoscopic radiofrequency ablation with the sector-ultrasonic probe (p). Puncture of the radiofrequency needle (r) was carried out under real-time ultrasonic guidance through the groove along the shaft of the sector probe. t, tumor. (f) Ultrasonographic image obtained by the sector ultrasonic probe. Radiofrequency needle was inserted along with the puncture guideline (arrow) into the tumor (arrowheads).

system (e.g. RITA Medical Systems, Inc., Mountain View, CA, USA)[27] or an internally water-cooled electrode with an impedance-controlled generator (e.g. Cool-tip system; Radionics, Burlington, MA, USA)[28] is used. The specification of these electrodes and generators has been discussed elsewhere.[27,28]

The main difficulty, as in all laparoscopic ultrasound-guided procedures, is the insertion of the needle into the lesion, because of the presence of a double fulcrum presented by the abdominal wall and the hepatic parenchyma. Specific expertise is necessary to avoid repeated passage of the needle. To prevent tumor dissemination, the RF needle should be inserted through normal liver tissue to avoid direct puncture of the tumor. Based on our experience, an endoretractor is useful to expose the tumor and to protect against visceral injury in the event that the tumor is located on the inferior surface, which is hidden by adjacent viscera. Other techniques reported in the literature include three-dimensional computed tomography to simulate the laparoscopic strategy (Fig. 1), the use of a cutter to remove adhered mesentery,[29] or a combination of hand-assisted laparoscopic surgery[30] and liver resection.[31]

ADVANTAGES OF THE LAPAROSCOPIC APPROACH

The laparoscopic approach offers the advantages of a minimally invasive procedure including direct visual control of the RFA procedure, exposure and isolation of the liver from the surrounding tissue, and the management of intraoperative complications.[25]

The treatment of a HCC on the superior or inferior surface of the liver can potentially ablate the adjacent abdominal wall or, worse, the adjacent viscera with the possibility of major post-procedure complications and tumor seeding.[32–34] Hence, the laparoscopic approach is well indicated in superficial or extrahepatic protrusive HCC, and HCC adjacent to the gastrointestinal tract, gallbladder, bile duct or heart.[35,36] In cases of paracholecystic HCC, the laparoscopic procedure allows for a cholecystectomy and enables a direct approach through the gallbladder fossa to ablate the tumor.[24,37] The laparoscopic approach with a positive-pressure pneumoperitoneum has a distinct advantage over the percutaneous approach because liver blood flow is reduced by approximately 40%.[38]

BENEFITS OF LAPAROSCOPIC ULTRASOUND

The laparoscopic approach also offers the ability to carry out an intraoperative high-frequency ultrasound examination. Using laparoscopic ultrasound during the procedure can help identify the treatable lesion, detect new HCC lesions that were not identified by preoperative imaging,[39–44] and aid RF-needle placement for more accurate targeting.[37,45–50] Initially, laparoscopy and laparoscopic ultrasound were found to be useful for staging and detecting new HCC that could not be identified preoperatively.[39–44,48] With advances in laparoscopic ultrasonographic probes, the role of laparoscopic RFA has become particularly important in the subdiaphragmatic area where percutaneous ultrasound has limited use for detecting tumors and increases the risk for diaphragmatic thermal injury.

With advances in technology, several types of laparoscopic ultrasonographic probes have been developed. The linear scan type, which was originally designed to assist during laparoscopic cholecystectomy, has been applied to laparoscopic RFA (e.g. flexible 7.5-MHz probe, Aloka Co., Tokyo, Japan; 7.5-MHz linear array probe, Hitachi Co., Tokyo, Japan and B&K Medical, Copenhagen, Denmark). Despite its good image resolution, a linear probe requires skill and experience,[45,51–53] or the development of special navigation technology,[47–50] to precisely target a tumor for ablation. This clinical obstacle has been overcome by new types of ultrasonic probes; the sector type (Aloka Co.)[37] and the convex scan type (PVM-787LA; Toshiba Medicals, Tokyo, Japan).[46] These probes are designed to target intrahepatic tumors because they have a guiding tract on the shaft that allows the user to see an ablation needle advancing into a tumor on a real-time ultrasonographic image. This feature has widened the indication for laparoscopic ablation in cases where tumors are located beneath the surface away from the direct view of the laparoscope.

EFFICACY AND PROGNOSIS

The overall local recurrence rate of RFA using the percutaneous and laparoscopic approaches varies from 1.8 to 14%.[54–59] The local recurrence rate of laparoscopic RFA varies from 0 to 12%.[22,24,37,40,46,52,53,60–63] Many of these studies have suggested that local control of the laparoscope is an advantage during laparoscopic RFA compared with the percutaneous approach. Reported factors associated with the risk of local recurrence include an HCC with multiple lesions, size >30 mm in diameter, infiltrative type, capsular invasion, vascular invasion and an inadequate ablation margin.[60,61,63] The risk of local recurrence increases with an increase in HCC size, but the local recurrence rate differs markedly if a circumferential 5-mm safety margin can be secured. In addition, risk factors associated with distant recurrence after RFA are multiple HCC and hepatitis C viral infection.[64]

Although the short history of RFA prevents an analysis of long-term prognosis, several reports have indicated a 3-year survival rate of 40–60%.[65,66] We found no local recurrence in our series of 84 patients with HCC who underwent curative laparoscopic RFA from 1999 as an initial therapy, whereas the 1-year local recurrence rate in patients treated with percutaneous RFA ($n = 485$) was 3.9%. The cumulative survival rates at 1, 3 and 5 years in patients with laparoscopic RFA as an initial therapy were 100%, 84% and 81%, respectively ($n = 84$), which was comparable to patients with percutaneous RFA (96%, 1 year; 83%, 2 years; and 61%, 3 years, $n = 485$) (Fig. 2). Similar to percutaneous RFA, survival after laparoscopic RFA was determined by Child–Pugh class and alpha fetoprotein (AFP) levels.[65] It must be emphasized that operator skill, securing a safety margin around the tumor, accurate evaluation of the therapeutic response and an aggressive treatment all closely affect the results.

SAFETY

Safety is one of the most important issues in minimally invasive therapies such as laparoscopic RFA. The rate of major complication for laparoscopic RFA is reported to be 3.8%,[66]

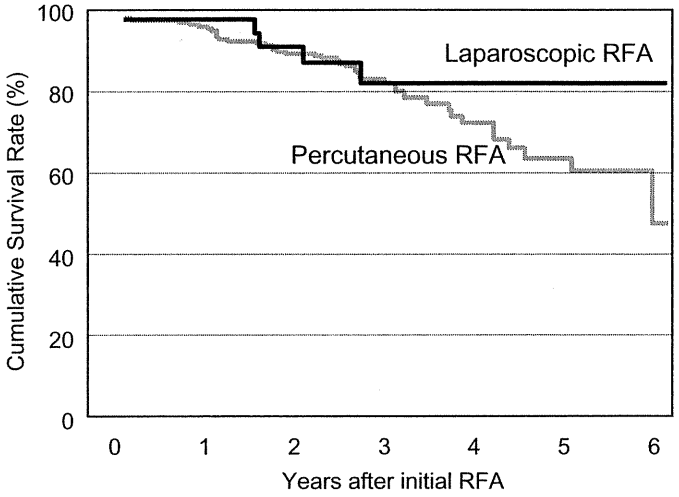

Fig. 2. Cumulative survival rate in patients with hepatocellular carcinoma who underwent laparoscopic (solid line, $n = 84$) or percutaneous (gray line, $n = 485$) radiofrequency ablation as an initial curative treatment in Musashino Red Cross Hospital from 1999.

which is lower than laparotomy,[62] transcatheter arterial chemoembolization[67] and percutaneous RFA.[68] Complications from laparoscopic RFA include liver failure, bile-duct thermal injury, liver abscess, pneumothorax, pneumonia, trocar injury involving the small bowel or gallbladder, postoperative bleeding from the mesentery, gastrointestinal bleeding, hepatic infarction, skin burns, pacemaker malfunction, congestive heart failure, hemoglobinuria and myoglobinuria.[61,62,67,69,70] Complications specific to laparoscopic RFA are pneumonia, pneumothorax, trocar injury and postoperative bleeding from the mesentery or abdominal wall. In our series of HCC patients who underwent laparoscopic RFA, 2.2% (2/92) had postoperative complications, which was comparable to the 2.0% (27/1333) observed for percutaneous RFA (Table 1).

In our experience, the use of a mesh-covered access port (VersaStep™) avoids trocar injury and bleeding from the mesentery and abdominal wall. The mandatory use of laparoscopic-ultrasound guidance during RF-needle puncture will avoid thermal injury to the intrahepatic vessels and/or bile duct and to adjacent organs such as the diaphragm, heart, gallbladder and intestine. Because patients with a history of biliopancreatic surgery have a higher rate of liver abscess formation,[66] special caution should be paid to these patients after the procedure.

CONCLUSION

Laparoscopic RFA is a safe and feasible treatment to cure an HCC tumor in selected patients. The main advantages of the laparoscopic approach are better neoplastic staging, and the ability to treat lesions for which percutaneous RFA is contraindicated or risky. The main disadvantages of this technique are the need to carry out the procedure under general anesthesia, its invasive nature compared with the percutaneous approach, and the risk of complications from the laparoscopy. Laparoscopic RFA should be considered complementary and not an alternative technique to percutaneous RFA. In order to define the indications for laparoscopic RFA, it is essential to develop considerable experience in the procedure and conduct clinical trials in comparison with other therapeutic techniques.

Table 1. Complications of laparoscopic and percutaneous radiofrequency ablation for hepatocellular carcinoma at the Musashino Red Cross Hospital

	Laparoscopic RFA $n = 92$	Percutaneous RFA $n = 1333$
Biliary fistula	0 (0%)	4 (0.30%)
Liver abscess	1 (1.1%)	4 (0.30%)
Intercostal arterial bleeding	0 (0%)	3 (0.22%)
Hemothorax	0 (0%)	2 (0.15%)
Liver infarction	0 (0%)	3 (0.22%)
Liver dysfunction	0 (0%)	2 (0.15%)
Tumor dissemination	0 (0%)	4 (0.30%)
Skin burn	0 (0%)	2 (0.15%)
Subcutaneous hematoma	1 (1.1%)	0 (0%)
Pneumothorax	0 (0%)	2 (0.15%)
Intestinal perforation	0 (0%)	1 (0.07%)
Total	2/92 (2.2%)	27/1333 (2.0%)

REFERENCES

1. El-serag HB, Mason AC. Rising incidence of hepatocellular carcinoma in the United States. *N. Engl. J. Med.* 1999; **340**: 745–50.
2. Taylor-Robinson SD, Foster GR, Arora S, Hargreaves S, Thomas HC. Increase in primary liver cancer in the UK, 1979–94. *Lancet* 1997; **350**: 1142–3.
3. Llovet JM, Burroughs A, Bruix J. Hepatocellular carcinoma. *Lancet* 2003; **362**: 1907–17.
4. Okuda K, Okuda H. Primary liver cell carcinoma. In: Mcintyre N, Benhamou JP, Bircher J, Rizzetto M, Rodes J (eds). *Oxford Textbook of Clinical Hepatology*, Vol. 2. Oxford: Oxford University Press, 1991; 1019–52.
5. Shiratori Y, Shiina S, Imamura M *et al.* Characteristic difference of hepatocellular carcinoma between hepatitis B- and C- viral infection in Japan. *Hepatology* 1995; **22**: 1027–33.
6. Yuen MF, Cheng CC, Lauder IJ, Lam SK, Ooi CG, Lai CL. Early detection of hepatocellular carcinoma increases the chance of treatment: Hong Kong experience. *Hepatology* 2000; **31**: 330–5.
7. Bruix J, Sherman M, Llovet JM *et al.* Clinical management of hepatocellular carcinoma. Conclusions of the Barcelona-2000 EASL conference. European Association for the Study of the Liver. *J. Hepatol.* 2001; **35**: 421–30.
8. Kudo M. Early detection and curative treatment of early-stage hepatocellular carcinoma. *Clin. Gastroenterol. Hepatol.* 2005; **3**: S144–8.
9. Ryder SD, British Society of Gastroenterology. Guidelines for the diagnosis and treatment of hepatocellular carcinoma (HCC) in adults. *Gut* 2003; **52**: iii1–8.
10. Llovet JM, Burroughs A, Bruix J. Hepatocellular carcinoma. *Lancet* 2003; **362**: 1907–17.
11. Balsells J, Charco R, Lazaro JL *et al.* Resection of hepatocellular carcinoma in patients with cirrhosis. *Br. J. Surg.* 1996; **83**: 758–61.

12. Mazzaferro V, Regalia E, Doci R *et al.* Liver transplantation for the treatment of small hepatocellular carcinomas in patients with cirrhosis. *N. Engl. J. Med.* 1996; **334**: 693–9.
13. Wall WJ, Marotta PJ. Surgery and transplantation for hepatocellular cancer. *Liver Transpl.* 2000; **6**: S16–22.
14. Vivarelli M, Bellusci R, Cucchetti A *et al.* Low recurrence rate of hepatocellular carcinoma after liver transplantation: Better patient selection or lower immunosuppression? *Transplantation* 2002; **74**: 1746–51.
15. Rossi S, Di Stasi M, Buscarini E *et al.* Percutaneous radio frequency interstitial thermal ablation in the treatment of small hepatocellular carcinoma. *Cancer J. Sci. Am.* 1995; **1**: 73–81.
16. Livraghi T, Goldberg SN, Lazzaroni S, Meloni F, Solbiati L, Gazelle GS. Small hepatocellular carcinoma: Treatment with radiofrequency ablation versus ethanol injection. *Radiology* 1999; **210**: 655–61.
17. Shiina S, Teratani T, Obi S, Hamamura K, Koike Y, Omata M. Nonsurgical treatment of hepatocellular carcinoma: From percutaneous ethanol injection therapy and percutaneous microwave coagulation therapy to radio frequency ablation. *Oncology* 2002; **62**: 64–8.
18. Lencioni RA, Allgaier HP, Cioni D *et al.* Small hepatocellular carcinoma in cirrhosis: Randomized comparison of radiofrequency thermal ablation versus percutaneous ethanol injection. *Radiology* 2003; **228**: 235–40.
19. Curley SA. Radiofrequency ablation of malignant liver tumors. *Oncologist* 2001; **6**: 14–23.
20. Bilchik AJ, Wood TF, Allegra DP. Radiofrequency ablation of unresectable hepatic malignancies: Lessons learned. *Oncologist* 2001; **6**: 24–33.
21. Curley SA, Davidson BS, Fleming RY *et al.* Laparoscopically guided bipolar radiofrequency ablation of areas of porcine liver. *Surg. Endosc.* 1997; **11**: 729–33.
22. Cuschieri A, Bracken J, Boni L. Initial experience with laparoscopic ultrasound-guided radiofrequency thermal ablation of hepatic tumours. *Endoscopy* 1999; **31**: 318–21.
23. Siperstein A, Garland A, Engle K *et al.* Laparoscopic radiofrequency ablation of primary and metastatic liver tumors. Technical considerations. *Surg. Endosc.* 2000; **14**: 400–5.
24. Goletti O, Lencioni R, Armillotta N *et al.* Laparoscopic radiofrequency thermal ablation of hepatocarcinoma: Preliminary experience. *Surg. Laparosc. Endosc. Percutan. Tech.* 2000; **10**: 284–90.
25. Topal B, Aerts R, Penninckx F. Laparoscopic radiofrequency ablation of unresectable liver malignancies: Feasibility and clinical outcome. *Surg. Laparosc. Endosc. Percutan. Tech.* 2003; **13**: 11–15.
26. Kudo M. Local ablation therapy for hepatocellular carcinoma: Current status and future perspectives. *J. Gastroenterol.* 2004; **39**: 205–14.
27. Patterson EJ, Scudamore CH, Buczkowski AK, Owen DA, Nagy AG. Radiofrequency ablation in surgery. *Surg. Technol. Int.* 1997; **6**: 69–75.
28. Francica G, Marone G. Ultrasound-guided percutaneous treatment of hepatocellular carcinoma by radiofrequency hyperthermia with a 'cooled-tip needle'. A preliminary clinical experience. *Eur. J. Ultrasound.* 1999; **9**: 145–53.
29. Kurokohchi K, Masaki T, Himoto T *et al.* Successful laparoscopic radiofrequency ablation of hepatocellular carcinoma adhered to the mesentery after transcatheter arterial embolization. *Oncol Rep* 2005; **13**: 65–8.
30. Ishiko T, Beppu T, Sugiyama S *et al.* Radiofrequency ablation with hand-assisted laparoscopic surgery for the treatment of hepatocellular carcinoma in the caudate lobe. *Surg. Laparosc. Endosc. Percutan. Tech.* 2008; **18**: 272–6.
31. Belli G, D'Agostino A, Fantini C *et al.* Laparoscopic radiofrequency ablation combined with laparoscopic liver resection for more than one HCC on cirrhosis. *Surg. Laparosc. Endosc. Percutan. Tech.* 2007; **17**: 331–4.
32. Stigliano R, Marelli L, Yu D, Davies N, Patch D, Burroughs AK. Seeding following percutaneous diagnostic and therapeutic approaches for hepatocellular carcinoma. What is the risk and the outcome? Seeding risk for percutaneous approach of HCC. *Cancer Treat. Rev.* 2007; **33**: 437–47.
33. Livraghi T, Solbiati L, Meloni MF, Gazelle GS, Halpern EF, Goldberg SN. Treatment of focal liver tumors with percutaneous radio-frequency ablation: Complications encountered in a multicenter study. *Radiology* 2003; **226**: 441–51.
34. Llovet JM, Vilana R, Brú C *et al.* Increased risk of tumor seeding after percutaneous radiofrequency ablation for single hepatocellular carcinoma. *Hepatology* 2001; **33**: 1124–9.
35. Yokoyama T, Egami K, Miyamoto M *et al.* Percutaneous and laparoscopic approaches of radiofrequency ablation treatment for liver cancer. *J. Hepatobiliary Pancreat. Surg.* 2003; **10**: 425–7.
36. Noguchi O, Izumi N, Kawamura H *et al.* Radiofrequency tumor ablation for hepatocellular carcinoma – Therapeutic significance of approaching methods and the device difference. *Jpn. J. Hyperthermia Oncol.* 2002; **18**: 21–30.
37. Noguchi O, Izumi N, Inoue K *et al.* Laparoscopic ablation therapy for hepatocellular carcinoma. Clinical significance of a newly developed laparoscopic sector ultrasonic probe. *Dig. Endosc.* 2003; **15**: 179–84.
38. Odeberg S, Ljungqvist O, Svenberg T *et al.* Haemodynamic effects of pneumoperitoneum and the influence of posture during anaesthesia for laparoscopic surgery. *Acta Anaesthesiol. Scand.* 1994; **38**: 276–83.
39. Montorsi M, Santambrogio R, Bianchi P *et al.* Laparoscopic radiofrequency of hepatocellular carcinoma (HCC) in liver cirrhosis. *Hepatogastroenterology* 2001; **48**: 41–5.
40. Chung MH, Wood TF, Tsioulias GJ, Rose DM, Bilchik AJ. Laparoscopic radiofrequency ablation of unresectable hepatic malignancies. A phase 2 trial. *Surg. Endosc.* 2001; **15**: 1020–6.
41. Montorsi M, Santambrogio R, Bianchi P *et al.* Radiofrequency interstitial thermal ablation of hepatocellular carcinoma in liver cirrhosis. Role of the laparoscopic approach. *Surg. Endosc.* 2001; **15**: 141–5.
42. Podnos YD, Henry G, Ortiz JA *et al.* Laparoscopic ultrasound with radiofrequency ablation in cirrhotic patients with hepatocellular carcinoma: Technique and technical considerations. *Am. Surg.* 2001; **67**: 1181–4.
43. Santambrogio R, Bianchi P, Palmisano A, Donadon M, Moroni E, Montorsi M. Radiofrequency of hepatocellular carcinoma in patients with liver cirrhosis: A critical appraisal of the laparoscopic approach. *J. Exp. Clin. Cancer. Res.* 2003; **22**: 251–5.
44. Ido K, Nakazawa Y, Isoda N *et al.* The role of laparoscopic US and laparoscopic US-guided aspiration biopsy in the diagnosis of multicentric hepatocellular carcinoma. *Gastrointest. Endosc.* 1999; **50**: 523–6.
45. Salmi A, Metelli F. Laparoscopic ultrasound-guided radiofrequency thermal ablation of hepatic tumors: A new coaxial approach. *Endoscopy* 2003; **35**: 802.
46. Inamori H, Ido K, Isoda N *et al.* Laparoscopic radiofrequency ablation of hepatocellular carcinoma in the caudate lobe by using a new laparoscopic US probe with a forward-viewing convex-array transducer. *Gastrointest. Endosc.* 2004; **60**: 628–31.
47. Hildebrand P, Kleemann M, Roblick UJ, Mirow L, Bürk C, Bruch HP. Technical aspects and feasibility of laparoscopic

ultrasound navigation in radiofrequency ablation of unresectable hepatic malignancies. *J. Laparoendosc. Adv. Surg. Tech. A* 2007; **17**: 53–7.
48. Lai EC, Tang CN, Ha JP, Tsui DK, Li MK. The evolving influence of laparoscopy and laparoscopic ultrasonography on patients with hepatocellular carcinoma. *Am. J. Surg.* 2008; **196**(5): 736–40.
49. Bao P, Sinha TK, Chen CC, Warmath JR, Galloway RL, Herline AJ. A prototype ultrasound-guided laparoscopic radiofrequency ablation system. *Surg. Endosc.* 2007; **21**: 74–9.
50. Raggi MC, Schneider A, Härtl F, Wilhelm D, Wirnhier H, Feussner H. A family of new instruments for laparoscopic radiofrequency ablation of malignant liver lesions. *Minim. Invasive Ther. Allied Technol.* 2006; **15**: 42–7.
51. Abe T, Shinzawa H, Wakabayashi H *et al.* Value of laparoscopic microwave coagulation therapy for hepatocellular carcinoma in relation to tumor size and location. *Endoscopy* 2000; **32**: 598–603.
52. Hildebrand P, Kleemann M, Roblick U, Mirow L, Birth M, Bruch HP. Laparoscopic radiofrequency ablation of unresectable hepatic malignancies: Indication, limitation and results. *Hepatogastroenterology* 2007; **54**: 2069–72.
53. Santambrogio R, Podda M, Zuin M *et al.* Safety and efficacy of laparoscopic radiofrequency ablation of hepatocellular carcinoma in patients with liver cirrhosis. *Surg. Endosc.* 2003; **17**: 1826–32.
54. Rossi S, Di Stasi M, Buscarini E *et al.* Percutaneous RF interstitial thermal ablation in the treatment of hepatic cancer. *AJR Am. J. Roentgenol.* 1996; **167**: 759–68.
55. Bowles BJ, Machi J, Limm WM *et al.* Safety and efficacy of radiofrequency thermal ablation in advanced liver tumors. *Arch. Surg.* 2001; **136**: 864–9.
56. Buscarini L, Buscarini E, Di Stasi M, Vallisa D, Quaretti P, Rocca A. Percutaneous radiofrequency ablation of small hepatocellular carcinoma: Long-term results. *Eur. Radiol.* 2001; **11**: 914–21.
57. Curley SA, Izzo F, Delrio P *et al.* Radiofrequency ablation of unresectable primary and metastatic hepatic malignancies: Results in 123 patients. *Ann. Surg.* 1999; **230**: 1–8.
58. Curley SA, Izzo F, Ellis LM, Nicolas Vauthey J, Vallone P. Radiofrequency ablation of hepatocellular cancer in 110 patients with cirrhosis. *Ann. Surg.* 2000; **232**: 381–91.
59. Wood TF, Rose DM, Chung M, Allegra DP, Foshag LJ, Bilchik AJ. Radiofrequency ablation of 231 unresectable hepatic tumors: Indications, limitations, and complications. *Ann. Surg. Oncol.* 2000; **7**: 593–600.
60. Santambrogio R, Opocher E, Costa M, Cappellani A, Montorsi M. Survival and intra-hepatic recurrences after laparoscopic radiofrequency of hepatocellular carcinoma in patients with liver cirrhosis. *J. Surg. Oncol.* 2005; **89**: 218–25.
61. Machi J, Uchida S, Sumida K *et al.* Ultrasound-guided radiofrequency thermal ablation of liver tumors: Percutaneous, laparoscopic, and open surgical approaches. *J. Gastrointest. Surg.* 2001; **5**: 477–89.
62. Topal B, Aerts R, Penninckx F. Laparoscopic radiofrequency ablation of unresectable liver malignancies: Feasibility and clinical outcome. *Surg. Laparosc. Endosc. Percutan. Tech.* 2003; **13**: 11–15.
63. Berber E, Siperstein A. Local recurrence after laparoscopic radiofrequency ablation of liver tumors: An analysis of 1032 tumors. *Ann. Surg. Oncol.* 2008; **15**(10): 2757–64.
64. Izumi N, Asahina Y, Noguchi O *et al.* Risk factors for distant recurrence of hepatocellular carcinoma in the liver after complete coagulation by microwave or radiofrequency ablation. *Cancer* 2001; **91**: 949–56.
65. Berber E, Rogers S, Siperstein A. Predictors of survival after laparoscopic radiofrequency thermal ablation of hepatocellular cancer: A prospective study. *Surg. Endosc.* 2005; **19**: 710–14.
66. Berber E, Siperstein AE. Perioperative outcome after laparoscopic radiofrequency ablation of liver tumors: An analysis of 521 cases. *Surg. Endosc.* 2007; **21**: 613–18.
67. Hsieh CB, Chang HM, Chen TW *et al.* Comparison of transcatheter arterial chemoembolization, laparoscopic radiofrequency ablation, and conservative treatment for decompensated cirrhotic patients with hepatocellular carcinoma. *World J. Gastroenterol.* 2004; **10**: 505–8.
68. Eisele RM, Schumacher G, Jonas S, Neuhaus P. Radiofrequency ablation prior to liver transplantation: Focus on complications and on a rare but severe case. *Clin. Transplant.* 2008; **22**: 20–8.
69. Topal B, Hompes D, Aerts R, Fieuws S, Thijs M, Penninckx F. Morbidity and mortality of laparoscopic vs. open radiofrequency ablation for hepatic malignancies. *Eur. J. Surg. Oncol.* 2007; **33**: 603–7.
70. Pang YY, Andrew YW. Hemoglobinuria during laparoscopic radiofrequency ablation of hepatocellular carcinoma. *J. Gastroenterol. Hepatol.* 2006; **21**: 1355.

日本肝臓学会コンセンサス神戸2009：C型肝炎の診断と治療

西口　修平　　泉　　並木　　日野　啓輔　　鈴木　文孝
熊田　博光　　伊藤　義人　　朝比奈靖浩　　田守　昭博
平松　直樹　　林　　紀夫　　工藤　正俊

「肝臓」第50巻　第11号（2009）別刷

＜特別寄稿＞

日本肝臓学会コンセンサス神戸2009：C型肝炎の診断と治療

西口　修平[1)*]　泉　並木[2)]　日野　啓輔[3)]　鈴木　文孝[4)]
熊田　博光[4)]　伊藤　義人[5)]　朝比奈靖浩[2)]　田守　昭博[6)]
平松　直樹[7)]　林　紀夫[7)]　工藤　正俊[8)]

索引用語：　C型慢性肝炎　診断　治療　ガイドライン

はじめに

わが国のC型肝炎の特徴は，欧米に比し高齢であり肝組織所見の進展例が多く，経過観察中に高率に肝癌が生じてくることである．このため，患者背景の異なる欧米のガイドライン[1)]はわが国では当てはまらない事項もあり，日本の患者の実態に即した独自のガイドラインの策定が必要である．このような指針を求めて，第45回日本肝臓学会総会（工藤正俊会長）において，C型肝炎（病態・診断・予後・治療）をテーマとしたコンセンサス　パネルディスカッションが開催された．すでに，第5回，第7回，第10回の日本肝臓学会大会においても，同一テーマで討議されているため，今回が4回目となる．エビデンスレベルが高く，発表者と座長のコンセンサスが得られた事項で有益な情報をInformative statementとし，推奨すべき指針をRecommendationとして取り上げた．エビデンスレベルが低いため欧米のガイドラインでは採用されていないか，発表者と座長の予備検討において全員の賛同が得られなかった事項については，アンサーパッドで学会参加者に意見を求めた．その際，回答者の2/3以上の承認が得られればConsensus Statementとして採用した．アンサーパッドの参加者は200人であり，内訳は内科医が88%，肝炎診療の経験年数が10年以上の医師が83%，肝臓学会専門医も83%を占めた．本稿では，紙面の都合でInformative statementやRecommendationは明記せず，パネルディスカッションにおいて活発な討議が行われ，結論が得られたConsensus Statementのみ全文を記載した．

1）兵庫医科大学内科学・肝胆膵科
2）武蔵野赤十字病院消化器科
3）川崎医科大学肝胆膵内科学
4）虎の門病院肝臓センター
5）京都府立医科大学消化器内科学
6）大阪市立大学肝胆膵病態内科学
7）大阪大学消化器内科学
8）近畿大学消化器内科学
*Corresponding author: nishiguc@hyo-med.ac.jp
＜受付日2009年9月16日＞＜採択日2009年9月17日＞

1）病態・診断・予後

1．C型肝炎の発症機序

C型肝炎ウイルス（HCV）の肝細胞への感染はHCV E2タンパクがCD81と結合することが必要であると報告されたが，その後scavenger receptor class B type I（SR-B1）やclaudin-1（CLDN1）といった宿主タンパクも関与することが示された．さらに2009年になってoccluding（OCLN）がHCV感染に不可欠であることが明らかとなった．興味深いことにCLDN1とOCLNはともにtight junctionに存在する分子であり，HCVが肝細胞に接着した後の細胞内への取り込みに重要であると考えられている．さらにCD81とOCLNはHCV感染の種特異性に関与する分子であることも示されている[2)]．

HCVの持続感染が成立するためには，宿主の自然免疫からの回避が必要である．最近，HCVによる自然免疫の抑制機構が明らかにされた．すなわち，複製中のHCV RNAの一部はPAMPとしてRIG-IやTLRに認識される．RIG-Iに認識されたシグナルはIPS-1を介して内因性のインターフェロン（IFN）シグナルを活性化する．産生されたIFNはIFNレセプターに結合してJak-STATシグナルを活性化してIFN応答遺伝子の発現を促す．しかし，HCV NS3/4A proteaseはIPS-1を断裂することでIFNシグナルを阻害しIFN産生を抑制する．また，HCVコアタンパクに誘導されるSOCS-3はJak-

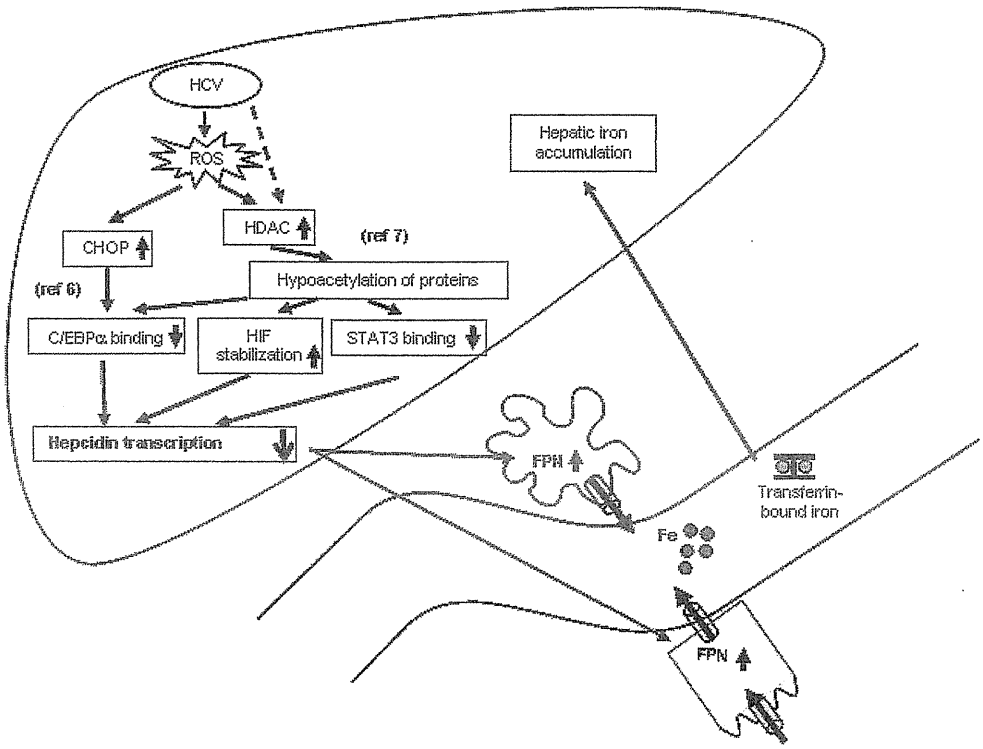

Fig. 1　Schematic diagram depicting the mechanisms underlying the hepatic iron accumulation induced by HCV
HCV-induced ROS reduces hepcidin transcription through the inhibited binding of CHOP and/or STAt3 to the hepcidin promoter, and/or stabilization of HIF that is negative hepcidin regulator.
HCV, hepatitis C virus; ROS, reactive oxygen species; HDAC, histone deacetylase; CHOP, C/EBP homology protein; C/EBP, CCAAT/enhancer-binding protein; HIF, hypoxia inducible factor; STAT, signal transducer and activation of transcription; FPN, ferroportin

STATシグナルを阻害してIFN応答遺伝子の発現を抑制し，NS5Aタンパクは IL-8の産生を亢進し，おそらくIFN応答遺伝子の発現を変化させることでIFNの抗ウイルス効果を減弱させる．更には，NS5AやE2タンパクはPKRに結合して，PKRの酵素活性を抑制することでIFNのウイルスタンパク翻訳抑制効果を阻害する[3]．HCVは以上に示したような様々な機構で宿主の自然免疫を回避すると考えられる．

HCVの持続感染成立後の肝細胞障害では，酸化ストレスが重要な役割を担っている．HCVコアタンパクはミトコンドリアを傷害し活性酸素を産生し肝臓に酸化ストレスを引き起こす[4][5]．さらにはTNFαやSOCS-3を介したinsulin receptor substrate（IRS）の抑制によるインスリン抵抗性の亢進，MTP抑制やSREBP1亢進による肝脂肪化，hepcidinの転写抑制を介した鉄蓄積などを引き起こし，C型肝炎に特徴的な病態を引き起こす（Fig. 1）[6][7]．これらの病態は肝発癌とも深く関連しており，さらにはペグインターフェロン（PEG-IFN）・リバビリン（RBV）併用療法の治療効果にも影響を与えることが報告されている．但し，肝内鉄過剰と抗ウイルス効果との関係については未だ一定の結論に至っていない．

Consensus Statement 1:

インスリン抵抗性と肝脂肪化はPEG-IFN・RBV併用療法の治療効果と関連する．(Level 2a, Grade C)

このようにC型肝炎の発症機序は次第に明らかにされつつあるが，肝発癌予測と抗ウイルス療法の効果予測に不可欠なのが肝線維化の評価である．最近ではelastographyを用いた非侵襲的な肝線維化の評価もなされているが，中等度の線維化の評価は未だ困難である．「肝線維化の評価のために肝生検は必要か？」という質